

Development of HfO_{2-x}-based Neural Memristor Utilizing Tantalum and Molybdenum Electrode

Kerem Karatas^{1,3*}, Bünyamin Özkal¹, Abdullah H. Cosar², Sinan Kazan¹

¹*Department of Physics, Gebze Technical University, Kocaeli, Turkiye*

²*Department of Materials Science, Gebze Technical University, Kocaeli, Turkiye*

³*Galatasaray University & Galatasaray High School, Istanbul, Turkiye*

ABSTRACT

In this research, we have fabricated a Ta/HfO_{2-x}/Mo-based single-cell memristor, a unique configuration worldwide. The synaptic behaviour of Tantalum and Molybdenum electrodes on an HfO_x-based memristor device has been investigated. HfO_{2-x} (15 nm) was grown using the Pulsed Laser Deposition (PLD) method, and electrodes were fabricated using a sputtering system and photolithography method. The metal oxide stoichiometry was ascertained via X-ray photoelectron spectroscopy (XPS). Long-term Potentiation (LTP) and paired pulsed facilitation (PPF) characteristics, which play a significant role in the learning processes of artificial neural networks, have been successfully obtained. Current-voltage measurements and retention tests were performed to determine the SET and RESET states of the device in appropriate ranges. The results show that this memristor device is a strong candidate for Artificial Neural Network (ANN) applications.

Keywords: Memristor, Synaptic Memristor, Resistive Switching HfO₂, Tantalum, Molybdenum, PLD.

*Corresponding author: kerem.karatas@galatasarayuniv.onmicrosoft.com

INTRODUCTION

Artificial Intelligence (AI) led to a white paper in science. AI's task definition aims to imitate the functionality of human intelligence and solve complex problems.[1] Including this definition; A significant amount of advantage is obtained in different fields such as automation & robots, the automotive industry, finance, healthcare, and daily basics.[2] Requested performances by AI require a high amount of energy, rapid processing, and massive data storage.[3] However, Inspecting through von Neumann Architecture, the foundational model of current computers needs to satisfy the requirements of low power consumption, high speed, and excessive data storage.[4-8] Because von Neumann Architecture separates the memory functions and computing processes, this causes complexity and a huge workload on the computers' Central Processing Unit (CPU).[9] Therefore, it is necessary to turn the tendency through neuromorphic computing. Neuromorphic computing is a method that aims to develop computer systems that can mimic the structure and functioning of the human brain. Imitation of the human brain allows us to replicate key brain functions such as learning, processing, analysing, and storing [10-12]. Artificial Neural Networks (ANNs) are crucial concepts to generate neuromorphic computing. These are models that simulate the brain's structure and function through layers of interconnected units called neurons. Biological neurons transmit electrical signals and connect with other neurons through synapses, forming the basis of learning and memory processes. Framing into these models, neuromorphic computing uses electrical devices to realize the human brain's functions as constituting neuron and synapse interactions [13-14].

Memristors are advanced and game-changer elements of neuromorphic computing. Memristors, initially proposed by Leon Chua in 1971 [15], are resistive switching devices capable of emulating synaptic functions, such as learning, memory retention, and adaptability. They possess essential characteristics for neuromorphic systems, including low power consumption, high speed, non-volatile memory, and multi-level data storage. These devices change their resistance states in response to electrical stimuli, allowing them to store and process information similarly to biological synapses. This

dynamic resistance adjustment enables memristors to replicate crucial processes of learning and adaptation, making them valuable for neuromorphic computing. [16-28]

HfO_{2-x} is worth investigating material in memristor production due to its distinctive characteristics. HfO_{2-x}-based memristors are best described by their scalability, stability (under different thermal and environmental conditions), controllability, and efficient resistive switching properties. [29-31] Its structure's deficiency allows us to get intended oxygen vacancies to realize memristive behaviours. Its analogue switching characteristics simulate the analogue nature of synapses, where the changes in resistance states imitate the synaptic weights. The configuration of HfO_{2-x} with metallic layers like Ta and Mo led to more facilitated and favored switching while decreasing the band gap value [32-38] thanks to their high oxidation [44] that can diffuse into the metal-oxide layer. Therefore, Ta/HfO_{2-x}/Mo is a worth exploring structure to get revolutionary steps in neuromorphic computing, respectively the future of AI.

In this work, we have fabricated and investigated the Ta/Pt/HfOx/Mo-based memristor device on a SiO₂ wafer. Ta and Mo electrodes were used as bottom and top electrodes fabricated by RF/DC magnetron sputter using standard photolithography technique for HfO_{2-x} based synaptic-memristor device. HfO_{2-x} layer was grown using the Pulsed Laser Deposition (PLD) technique. In this technique, high-k oxide materials are used as a single crystal target, allowing for easier crystalline film obtaining (causing Laser can vapors nanoparticles from the target) in a thin film on the substrate than other growth methods at optimum oxygen [45] and substrate temperature [46] values. Using X-ray photoelectron spectroscopy (XPS), the stoichiometry of the HfOx was examined. Memristive behaviour has been performed by the electrical characterization of Ta/HfO_{2-x}/Mo memristor, which showed nonlinear current-voltage (I-V) curves with a constricted hysteresis loop. The device's capacity to transition between a high resistance state (HRS) and a low resistance state (LRS) is necessary for both artificial synapse and memory applications. The retention tests further highlighted the device's potential for long-term data storage by showing it could sustain steady LRS and HRS values over time. These devices can also be used in neuromorphic systems, where they can mimic the plasticity of biological synapses and allow AI systems to perform advanced cognitive functions, thanks to the observation of long-term depression (LTD) and long-term potentiation (LTP) synaptic behaviours in these systems.

EXPERIMENTAL

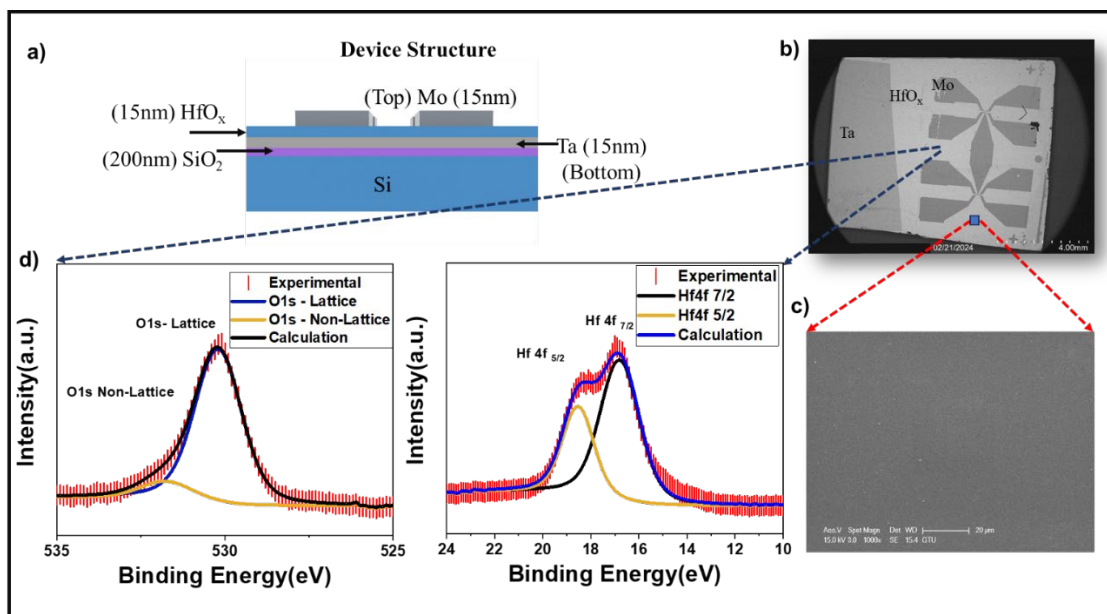


Figure 1: a) Device structure, b-c) SEM image of device (label 4 mm) and and HfOx surface (label 20 μm), d) The sample's XPS spectra for O1s (Left) and Hf4f (Right) are shown.

High-resolution (Phoibos 100, SPECS GmbH, Berlin, Germany) spectroscopy has been utilized to examine the stoichiometry and degree of oxidation of the deposited layers on the sample surface. Figure 1d provides a detailed investigation of the Hf 4f and O1s peaks. Based on the XPS spectrum, the observed Hf 4f doublet peaks at 16.9 eV (4f 7/2) and 18.5 eV (4f 5/2) indicate a role of Hf 4f in HfO_{2-x} . In equivalent XPS of HfO_2 data, a spin-orbit coupling of 1.6 eV was found. [35-36]. This peak was identified as the lattice and non-lattice oxygen, with binding energies of 530.3 and 531.8 eV, respectively, based on the best fitting of the O1s spectra. The computation result yields around 42% Hf and 58% O for HfO_{2-x} , indicating the growth oxide's stoichiometry.

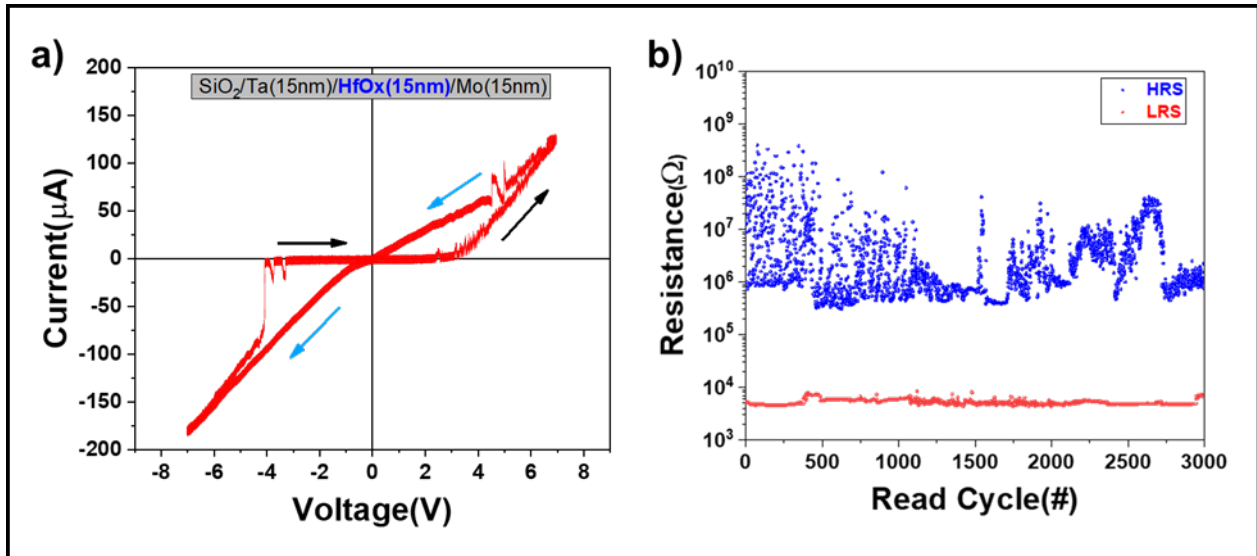


Figure 2: a) Current – voltage curve of device, b) Retention test for HRS and LRS with 3000 reads (1 V_{read}).

The pinched hysteresis loop is an indicator figure of memristor devices.[15] It barely shows SET and RESET passages of the memristor in current-voltage (I-V) graphs with linear sweeping voltages. The scan sequence was $0 \rightarrow +7.5 \text{ V} \rightarrow 0 \rightarrow -7.5 \text{ V} \rightarrow 0$. Directional mark 1 is the sequence of tracing SET voltage, the applied voltage that switches the memristor to LRS. Directional marks 2 and 3 are the sequences of RESET voltage, the applied voltage that switches the memristor from LRS to HRS. Directional mark 4 is the complementary part of the rest of the graph in HRS. In overall observation, the memristor changed its state while positive sweeping voltages, from HRS to LRS. When negative sweeping voltages were applied, the memristor switched to HRS.

The resistive switching system of memristors makes them special because memristors can switch between a High Resistance State (HRS) and a Low Resistance State (LRS) [39]. HRS comprises the conductive bridge formed by the arrangement of oxygen vacancies between two electrodes – Ta and Mo – is destructured. HRS is a static state, not requiring a continuous power supply; thus it is valuable for data retention. On the other hand, LRS is generated when the arrangement of oxygen vacancies between Ta and Mo electrodes constructs the conductive bridge. LRS consumes much more energy than HRS because of the free-flowing current. Experimental observation of these states separately is crucial for computational systems. HRS is the (RESET)off-state, 0 in the binary data storage system while (SET) LRS is the on-state, 1 in the binary data storage system.[40] The figure shows the resistance values in SET and RESET states where they're read 3000 times with a reading voltage of 1V.

In Figure 2a, when voltage was applied to the device from the top electrode (Mo), it had resistance on the order of $\text{k}\Omega$ up to around 3V. Although the HfO_{2-x} material has high oxygen defects, it is thought to be effective on the applied electric field due to the oxidation of the two oxidizable materials used. As a result, oxygen defects and Mo ions can move more slowly through the oxide material toward the

bottom electrode. It is observed that when the voltage reaches high values, the space charge limited current (SCLC) mechanism clearly dominates. Linear behaviour was observed both in the positive 6 and 7 and negative (-6 and -7) volt range. Around -4 volts, the device exhibited a successful memristor characteristic by switching to a high resistance state with a sharp inrush current drop. In addition, as shown in Figure 2b, it maintained the LRS state and HRS state stably, and from this graph, the R_{off}/R_{on} value was determined to be approximately 107.

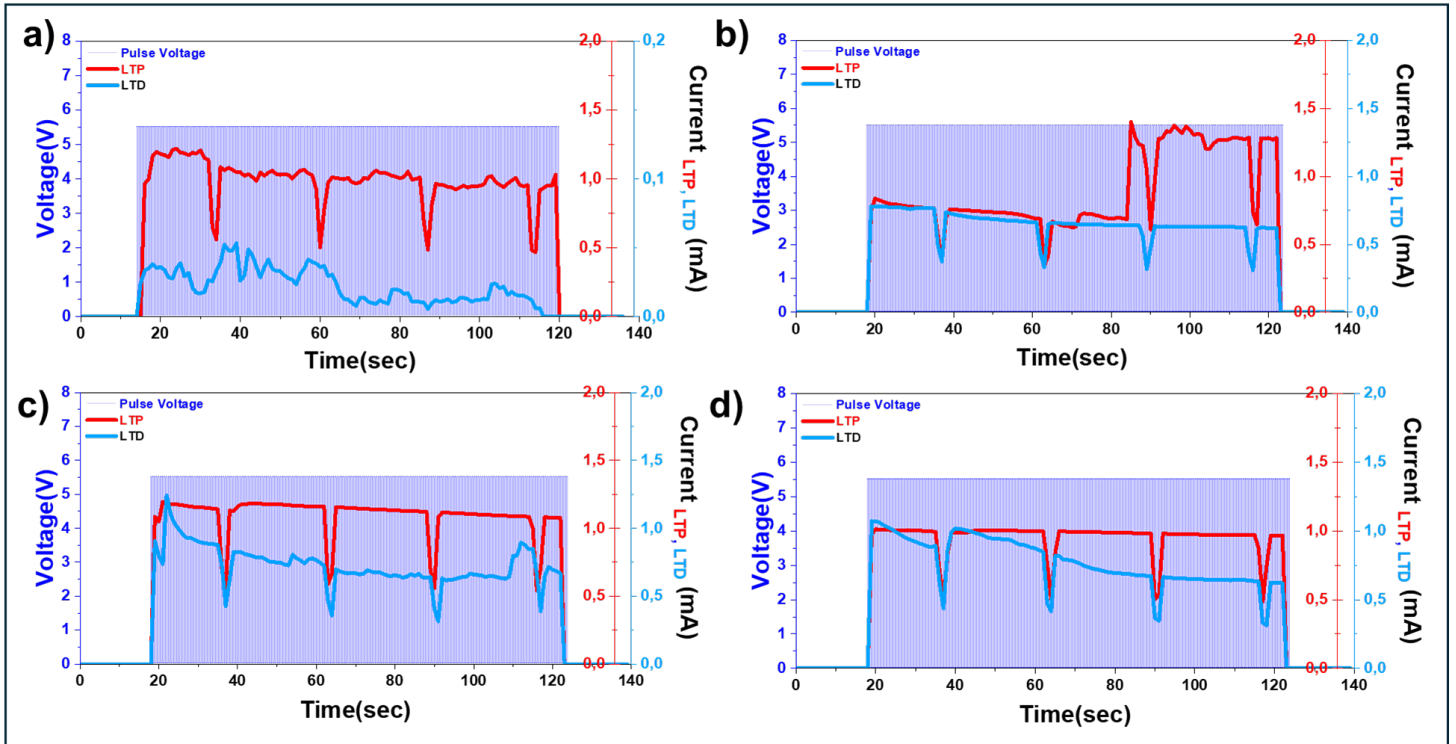


Figure 3: a-d) Measurement of four consecutive LTP and LTD devices with 300 pulses

Synaptic plasticity is the capability of changing in strength of synapses, depending on neural activity. This reflex allows for learning, memory, and adaptation skills in the human brain.[21] The synaptic weight defines the strength between synapses. If the synaptic weight increases, it means Long Term Potentiation (LTP) phase, and it refers to learning and memory nascency. On the other hand, a decrease in synaptic weight means Long Term Depression (LTD), and it refers to weakening the memory nascency – forgetting [41]. Firstly, 300 pulses were applied with an amplitude of 5.5 V. The Pulse period was 300 ms and the pulse width was 290 ms. Then, 300 more pulses were applied with an amplitude of -5.5 V in the same pulse period and width. These steps allowed us to observe average maximum and minimum limits' variation between given 5.5V voltage and read voltages pulse by pulse. That shows us the synaptic reactions of the memristor to the given electric stimulus. Positive pulses led the device to the LTP – learning and memory phase; while negative pulses led to the LTD – forgetting and weakening of memory phase [41]. This type of synaptic measurement is made 5 times to demonstrate the stability of the Ta/HfO_{2-x}/Mo-based memristors' neural characteristics.

In subsequent synaptic measurements, the device showed fast switching characteristics, switching from a low resistance state to around 5 pulses on average. This result shows that the device can switch within milliseconds and successfully keeps the conductance states.

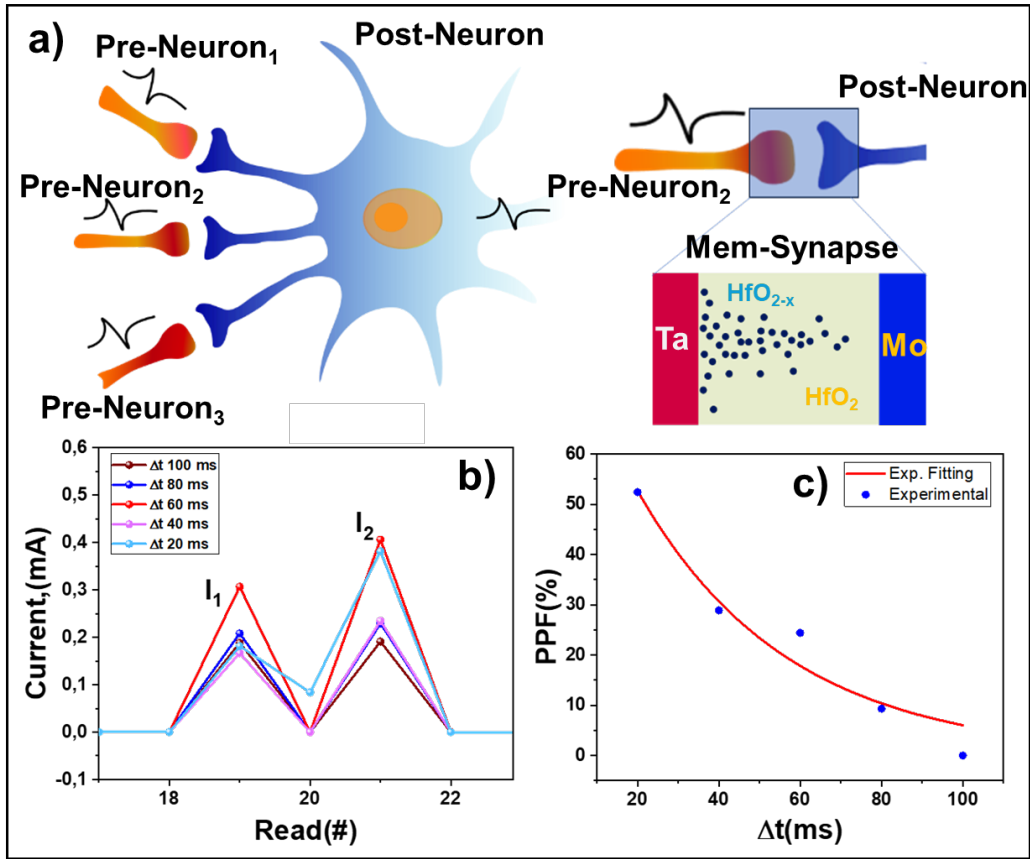


Figure 4: a) Interconnected neurons and the memristor analogy., b-c) PPF measurement of device.

Paired-pulse facilitation (PPF) is a process that simulates the time course of synaptic efficacy, and memristors can mimic this synaptic behavior.[42] The change in PPF percentage is representative of natural synaptic functioning and shows the temporal trend of the signal occurring across synapses. In that way, 2 pulses were applied with an amplitude of 5.5 V to the memristor with a constant pulse period of 300 ms. However, the pulse width is decreased by 20 for 5 times. Increasing the difference between the pulse period and width means the time difference between two consecutive stimuli, Δt . If t increases, the intensity of the second pulse will be less. Because, after the first pulse is applied, the carrier charges between the electrodes in the memristor and the ions remain active. However, these carrier charges and the effects of the ions on the memristor become passive over time after the applied stimulus. At this point, the shorter the time between the first and second pulses, the more the carrier charges and ions create a stimuli intensity on top of the effect that is produced by the active carrier.[43] This also shows that if Δt decreases, the stimulus intensity increases. Experimentally, this situation is shown sequentially as a current pulse diagram as seen in Figure 4b. The experimental output obtained in Figure A is numerically plotted as PPF percentage in Figure 4c. At this point, the PPF percentage decreases exponentially compared to Δt .

$$PPF\% = y = ae^{-\frac{\Delta t}{\tau}}$$

$$a = 90.53 \quad \tau = 36.955 \text{ ms}$$

This formula represents the exponential fit of PPF percentage graph respected to experimental data. "a" is fitting coefficient while τ is response time of the setup.

Device Fabrication

Photolithography, DC sputter, and PLD thin-film manufacturing have been used in the device's fabrication. The MBJ04 mask aligner has been used with AZ 1505 positive photoresist and a chrome mask to obtain the Mo top electrode (TE) lithographically. BE with a 15 nm Ta size was produced on a thermally oxidized Si substrate in a high-vacuum sputter chamber operating at 5×10^{-3} mbar Ar pressure at ambient temperature. A 15 nm HfO_{2-x} metal oxide layer is formed using a 350 mJ and 10 Hz pulse KrF (248 nm) laser (Compex 205) Pulse Laser Deposition (PLD) system at ambient temperature following a comparable second layer photolithography technique. The top electrode (TE) underwent final photolithography, and 15 nm Mo was deposited in the sputter. Lithography steps included photoresist removal with acetone and cleaning techniques. The devices are inspected using a Hitachi TM4000Plus scanning electron microscopy (SEM) system at various fabrication phases. The SEM and picture of the last device used in this work are shown in Figures 1b, c, emphasizing the areas that overlapped for the electrical measurements. The finished thin film stack and the device geometry are shown in Figure 1a.

Electrical Characterization.

In this study, a Keithley 2450 source meter and an AFG 31102 model Arbitrary Function Generator (AFG) were used to measure the DC transport Figure 2, LTP, LTD, and PPF of the memristor. To the upper electrode of the memristor, Mo, is connected to the positive (and negative outputs) to be applied 5.5V (and -5.5 V) pulses respectively. Instantaneous passing current through the memristor is read by the Keithley 2450 source-meter.

CONCLUSION

In this study, a memristor device in Ta/HfO_x/Mo structure was fabricated by Magnetron Sputter and PLD, and presented with an SEM image. Oxygen defects, which are important for memristor devices, were determined by the Hf/O ratio using the XPS method. Memristive characteristics and retention values were determined by DC transport measurement. In addition, LTP-LTD and PPF measurements were taken and synaptic characteristics were determined. As a result, the effects of the two oxidizable materials for the memristor device have been successfully demonstrated on both their synaptic properties and their stability in resistance states.

Acknowledgment

This work was supported by the Scientific and Technical Research Council of Turkey (TUBITAK) through the project project No. 121F390.

Author contributions:

SK, BÖ and KK conceived of the presented idea. SK, BÖ and KK verified the analytical methods. Device has been fabricated by BÖ and KK . BÖ carried out the X-Ray photoelectron spectroscopy studies of the samples. AHC carried out device image by SEM. KK have all carried out electrical and synaptic measurements. Everyone who wrote a piece of the final manuscript discussed the outcomes.

Conflicts of interest: All authors declare that they have no conflicts of interest.

Data and code availability: All data produced by authors are presented in this manuscript and they are available in DOI:

Supplementary information: There is no any additional material omitted from the main body of the text.

Ethical approval: Ethical approval is not applicable, because this article does not contain any studies with human or animal subjects.

ORCID iDs

Kerem Karataş : <https://orcid.org/0009-0002-5834-2428>

Bünyamin Özkal : <https://orcid.org/0000-0002-9964-9250>

Abdullah H. Coşar : <https://orcid.org/0009-0000-5273-5736>

Sinan Kazan : <https://orcid.org/0000-0002-8183-5733>

REFERENCES

- [1] Fan, Jingtao, et al. "From Brain Science to Artificial Intelligence." *Engineering*, vol. 6, no. 3, 2020, pp. 248-252. *ScienceDirect*, <https://doi.org/10.1016/j.eng.2019.11.012>
- [2] Soori, M., Arezoo, B., & Dastres, R. (2023). Artificial intelligence, machine learning and deep learning in advanced robotics, a review. In *Cognitive Robotics* (Vol. 3, pp. 54–70). KeAi Communications Co. <https://doi.org/10.1016/j.cogr.2023.04.001>
- [3] Zhang, J., and D. Tao. "Empowering Things With Intelligence: A Survey of the Progress, Challenges, and Opportunities in Artificial Intelligence of Things." *IEEE Internet of Things Journal*, vol. 8, no. 10, 15 May 2021, pp. 7789-7817, <https://doi.org/10.1109/JIOT.2020.3039359>
- [4] He, Weifan, et al. "Customized Binary and Multi-Level HfO₂-x-Based Memristors Tuned by Oxidation Conditions." *Scientific Reports*, vol. 7, no. 1, 30 Aug. 2017, p. 10070. *Nature*, <https://doi.org/10.1038/s41598-017-09413-9>
- [5] Zhu, Jiadi, Teng Zhang, Yuchao Yang, and Ru Huang. "Memristor-Based Artificial Synapses and Neuromorphic Systems." *Applied Physics Reviews*, vol. 7, no. 1, 2020, p. 011312, <https://doi.org/10.1063/1.5118217>
- [6] Mead, C. "Neuromorphic Electronic Systems." *Proceedings of the IEEE*, vol. 78, no. 10, 1990, pp. 1629-1636, <https://doi.org/10.1109/5.58356>
- [7] Burr, Geoffrey W., et al. "Emerging Materials in Neuromorphic Computing: Guest Editorial." *APL Materials*, vol. 8, no. 1, 2020, p. 010401, <https://doi.org/10.1063/1.5143659>
- [8] Davies, M., et al. "Advancing Neuromorphic Computing With Loihi: A Survey of Results and Outlook." *Proceedings of the IEEE*, vol. 109, no. 5, May 2021, pp. 911-934, <https://doi.org/10.1109/JPROC.2021.3067593>.
- [9] Zou, X., S. Xu, X. Chen, et al. "Breaking the von Neumann Bottleneck: Architecture-Level Processing-in-Memory Technology." *Science China Information Sciences*, vol. 64, 2021, p. 160404, <https://doi.org/10.1007/s11432-020-3227-1>
- [10] van de Burgt, Y., Melianas, A., Keene, S. T., et al. "Organic Electronics for Neuromorphic Computing." *Nature Electronics*, vol. 1, no. 6, 2018, pp. 386–397. <https://doi.org/10.1038/s41928-018-0103-3>
- [11] Furber, Steve. "J. Neural Eng. 13 051001." *Journal of Neural Engineering*, vol. 13, no. 5, 2016, IOP Publishing Ltd, <https://doi.org/10.1088/1741-2560/13/5/051001>
- [12] Burr, G. W., Shelby, R. M., Sebastian, A., Kim, S., Sidler, S., et al. "Neuromorphic Computing Using Non-Volatile Memory." *Advances in Physics: X*, vol. 2, no. 1, 2016, pp. 89–124. <https://doi.org/10.1080/23746149.2016.1259585>

- [13] Tian, Changfa, Wei, Liubo, Li, Yanran, and Jiang, Jie. "Recent Progress on Two-Dimensional Neuromorphic Devices and Artificial Neural Network." *Current Applied Physics*, vol. 31, 2021, pp. 182–198. <https://doi.org/10.1016/j.cap.2021.08.014>
- [14] Fu, J., Liao, Z., and Wang, J. "Memristor-Based Neuromorphic Hardware Improvement for Privacy-Preserving ANN." *IEEE Transactions on Very Large Scale Integration (VLSI) Systems*, vol. 27, no. 12, Dec. 2019, pp. 2745–2754. <https://doi.org/10.1109/TVLSI.2019.2923722>
- [15] Chua L 1971 Memristor the missing circuit element *IEEE Trans. Cir. Theory* 18 507519.
- [16] Strukov, D., Snider, G., Stewart, D., et al. "The Missing Memristor Found." *Nature*, vol. 453, 2008, pp. 80–83. <https://doi.org/10.1038/nature06932>
- [17] Bégon-Lours, L., Halter, M., Popoff, Y., & Offrein, B. J. (2021). Ferroelectric, Analog Resistive Switching in Back-End-of-Line Compatible TiN/HfZrO₄/TiO_x Junctions. *Physica Status Solidi - Rapid Research Letters*, 15(5). <https://doi.org/10.1002/pssr.202000524>
- [18] Ekinci, G., et al. (2024). "Investigation of Resistance Switching and Synaptic Properties of VO_x for Neuromorphic Applications." *ACS Omega* 9(24): 26235-26244.
- [19] Chen, Z., Lin, Z., Yang, J., Chen, C., Liu, D., Shan, L., Hu, Y., Guo, T., & Chen, H. (2024). Cross-layer transmission realized by light-emitting memristor for constructing ultra-deep neural network with transfer learning ability. *Nature Communications*, 15(1). 8 <https://doi.org/10.1038/s41467-024-46246-3>
- [20] Gier, C., Ben Yaala, M., Wiseman, C., MacFoy, S., Chicoine, M., Schiettekatte, F., Hough, J., Rowan, S., Martin, I., MacKay, P., & Reid, S. (2023, April). Controlling the optical properties of hafnium dioxide thin films deposited with electron cyclotron resonance ion beam deposition. *Thin Solid Films*, 771, 139781. <https://doi.org/10.1016/j.tsf.2023.139781>
- [21] Thomas, Andy. "Memristor-Based Neural Networks." *Journal of Physics D: Applied Physics*, vol. 46, no. 9, 2013, IOP Publishing Ltd. <https://doi.org/10.1088/0022-3727/46/9/093001>
- [22] Yao, P., Wu, H., Gao, B. *et al.* Fully hardware-implemented memristor convolutional neural network. *Nature* **577**, 641–646 (2020). <https://doi.org/10.1038/s41586-020-1942-4>
- [23] Li, Yibo, et al. "Review of Memristor Devices in Neuromorphic Computing: Materials Sciences and Device Challenges." *Journal of Physics D: Applied Physics*, vol. 51, no. 50, 2018, IOP Publishing Ltd. <https://doi.org/10.1088/1361-6463/aade3f>
- [24] Kim, H., Sah, M. P., Yang, C., Roska, T., and Chua, L. O. "Memristor Bridge Synapses." *Proceedings of the IEEE*, vol. 100, no. 6, June 2012, pp. 2061–2070. <https://doi.org/10.1109/JPROC.2011.2166749>
- [25] Chen, Jianbiao, et al. "High-Performance Memristor Based on MoS₂ for Reliable Biological Synapse Emulation." *Materials Today Communications*, vol. 32, 2022, 103957. <https://doi.org/10.1016/j.mtcomm.2022.103957>
- [26] Ismail, M., Rasheed, M., Mahata, C. *et al.* Mimicking biological synapses with a-HfSiO_x-based memristor: implications for artificial intelligence and memory applications. *Nano Convergence* **10**, 33 (2023). <https://doi.org/10.1186/s40580-023-00380-8>
- [27]] Guo, Y., Duan, W., Liu, X., Wang, X., Wang, L., Duan, S., Ma, C., & Li, H. (2023). Generative complex networks within a dynamic memristor with intrinsic variability. *Nature Communications*, 14(1). <https://doi.org/10.1038/s41467-023-41921-3>
- [28] Li, C., Belkin, D., Li, Y. *et al.* Efficient and self-adaptive in-situ learning in multilayer memristor neural networks. *Nat Commun* **9**, 2385 (2018). <https://doi.org/10.1038/s41467-018-04484-2>

- [29] Cheynet, M. C., Pokrant, S., Tichelaar, F. D., & Rouvière, J. L. (2007, March 1). Crystal structure and band gap determination of HfO₂ thin films. *Journal of Applied Physics*, 101(5).
<https://doi.org/10.1063/1.2697551>
- [30] Zhang, L., Liu, M., Ren, W., Zhou, Z., Dong, G., Zhang, Y., Peng, B., Hao, X., Wang, C., Jiang, Z. D., Jing, W., & Ye, Z. G. (2017). ALD preparation of high-k HfO₂ thin films with enhanced energy density and efficient electrostatic energy storage. *RSC Advances*, 7(14), 8388–8393.
<https://doi.org/10.1039/c6ra27847g>
- [31] Zhong, Y., Tang, J., Li, X., Gao, B., Qian, H., & Wu, H. (2021). Dynamic memristor-based reservoir computing for high-efficiency temporal signal processing. *Nature Communications*, 12(1).
<https://doi.org/10.1038/s41467-020-20692-1>
- [32] Ryu, H., & Kim, S. (2020, August 7). Pseudo-Interface Switching of a Two-Terminal TaOx/HfO₂ Synaptic Device for Neuromorphic Applications. *Nanomaterials*, 10(8), 1550.
<https://doi.org/10.3390/nano10081550>
- [33] Kim, Gil Seop, et al. "Defect-Engineered Electroforming-Free Analog HfOx Memristor and Its Application to the Neural Network." *ACS Applied Materials & Interfaces*, vol. 11, no. 50, 2019, pp. 47063–47072. <https://doi.org/10.1021/acsami.9b16499>.
- [34] Saleem, Aftab, et al. "Oxygen vacancy transition in HfOx-based flexible, robust, and synaptic Bi-layer memristor for neuromorphic and wearable applications." *Advanced Materials Technologies* 7.7 (2022): 2101208
- [35] Jiang, H., Han, L., Lin, P., Wang, Z., Jang, M. H., Wu, Q., Barnell, M., Yang, J. J., Xin, H. L., & Xia, Q. (2016). Sub-10 nm Ta Channel Responsible for Superior Performance of a HfO₂ Memristor. *Scientific Reports*, 6. <https://doi.org/10.1038/srep28525>
- [36] Özkal, B., Kazan, S., Karataş, Ö., Ekinci, G., Arda, L., & Rameev, B. Z. (2023). Fabrication and characterization of TiOx based single-cell memristive devices. *Materials Research Express*, 10(12).
<https://doi.org/10.1088/2053-1591/ad1125>
- [37] Lee, Daeseok, et al. "Dependence of Reactive Metal Layer on Resistive Switching in a Bi-Layer Structure Ta/HfOx Filament Type Resistive Random Access Memory." *Applied Physics Letters*, vol. 104, 2014, 083507. <https://doi.org/10.1063/1.4866671>
- [38] Liang, Y., Lu, Z., Wang, G., Yu, D., and Lu, H. H.-C. "Threshold-Type Binary Memristor Emulator Circuit." *IEEE Access*, vol. 7, 2019, pp. 180181–180193. <https://doi.org/10.1109/ACCESS.2019.2957371>
- [39] Fadeev, A.V., Rudenko, K.V. To the Issue of the Memristor's HRS and LRS States Degradation and Data Retention Time. *Russ Microelectron* 50, 311–325 (2021).
<https://doi.org/10.1134/S1063739721050024>
- [40] Liang, Y., Lu, Z., Wang, G., Yu, D., and Lu, H. H.-C. "Threshold-Type Binary Memristor Emulator Circuit." *IEEE Access*, vol. 7, 2019, pp. 180181–180193. <https://doi.org/10.1109/ACCESS.2019.2957371>
- [41] Kim, H., Sah, M. P., Yang, C., Roska, T., and Chua, L. O. "Neural Synaptic Weighting With a Pulse-Based Memristor Circuit." *IEEE Transactions on Circuits and Systems I: Regular Papers*, vol. 59, no. 1, Jan. 2012, pp. 148–158. <https://doi.org/10.1109/TCSI.2011.2161360>
- [42] Hu, S. G., et al. "Emulating the Paired-Pulse Facilitation of a Biological Synapse with a NiOx-Based Memristor." *Applied Physics Letters*, vol. 102, 2013, 183510. <https://doi.org/10.1063/1.4804374>

[43] Wang, Ruopeng, et al. "Recent Advances of Volatile Memristors: Devices, Mechanisms, and Applications." *Advanced Intelligent Systems*, first published 8 July 2020, <https://doi.org/10.1002/aisy.202000055>

[44] University of Cambridge. "Ellingham Diagrams." DoITPoMS, University of Cambridge, https://www.doitpoms.ac.uk/tlplib/ellingham_diagrams/index.php Accessed 3 Aug. 2024.

[45] Makarov, G. N. "Laser Applications in Nanotechnology: Nanofabrication Using Laser Ablation and Laser Nanolithography." *Physics-Uspekhi*, vol. 56, no. 7, 2013, pp. 643-673, Russian Academy of Sciences, <https://doi.org/10.3367/UFNe.0183.201307a.0673>

[46] Beena, D., et al. "Effect of Substrate Temperature on Structural, Optical and Electrical Properties of Pulsed Laser Ablated Nanostructured Indium Oxide Films." *Applied Surface Science*, vol. 255, no. 20, 2009, pp. 8334-8342, <https://doi.org/10.1016/j.apsusc.2009.05.057>